Contrib Mineral Petrol (2016) 171:39
DOI 10.1007/s00410-016-1245-9

ORIGINAL PAPER

Compositional variations in spinel-hosted pargasite inclusions in the olivine-rich rock from the oceanic crust–mantle boundary zone

Akihiro Tamura[1] · Tomoaki Morishita[1] · Satoko Ishimaru[2] · Kaori Hara[1] · Alessio Sanfilippo[1,3] · Shoji Arai[1]

Received: 26 November 2014 / Accepted: 20 February 2016 / Published online: 15 April 2016

Abstract The crust–mantle boundary zone of the oceanic lithosphere is composed mainly of olivine-rich rocks represented by dunite and troctolite. However, we still do not fully understand the global variations in the boundary zone, and an effective classification of the boundary rocks, in terms of their petrographical features and origin, is an essential step in achieving such an understanding. In this paper, to highlight variations in olivine-rich rocks from the crust–mantle boundary, we describe the compositional variations in spinel-hosted hydrous silicate mineral inclusions in rock samples from the ocean floor near a mid-ocean ridge and trench. Pargasite is the dominant mineral among the inclusions, and all of them are exceptionally rich in incompatible elements. The host spinel grains are considered to be products of melt–peridotite reactions, because their origin cannot be ascribed to simple fractional crystallization of a melt. Trace-element compositions of pargasite inclusions are characteristically different between olivine-rich rock samples, in terms of the degree of Eu and Zr anomalies in the trace-element pattern. When considering the nature of the reaction that produced the inclusion-hosting spinel, the compositional differences between samples were found to reflect a diversity in the origin of the olivine-rich rocks, as for example in whether or not a reaction was accompanied by the fractional crystallization of plagioclase. The differences also reflect the fact that the melt flow system (porous or focused flow) controlled the melt/rock ratios during reaction. The pargasite inclusions provide useful data for constraining the history and origin of the olivine-rich rocks and therefore assist in our understanding of the crust–mantle boundary of the oceanic lithosphere.

Keywords Pargasite inclusion · Dunite · Troctolite · Trace-element pattern · Melt–peridotite reaction

Communicated by Othmar Müntener.

✉ Akihiro Tamura
aking826@staff.kanazawa-u.ac.jp

[1] Department of Earth Sciences, Kanazawa University, Kakuma, Kanazawa 920-1192, Japan

[2] Department of Earth and Environmental Sciences, Kumamoto University, Kurokami, Chuo-ku, Kumamoto 860-8555, Japan

[3] Present Address: Dipartimento di Scienze della Terra e dell'Ambiente, Università degli Studi di Pavia, Via Ferrata, 9, 27100 Pavia, Italy

Introduction

Petrological studies of rocks from ophiolites and modern oceanic spreading centers have revealed that the crust–mantle boundary zone of oceanic lithosphere is composed mainly of olivine-rich rocks such as troctolite and dunite (e.g., Nicolas 1989; Arai and Matsukage 1996; Dick and Natland 1996). In contrast to the well-ordered lithological sequence observed in the Oman ophiolite, which is an analog of a fast-spreading ridge system, the structure of a slow-spreading oceanic lithosphere is expected to be more variable and complicated, with perhaps a lack of crust or an ambiguous crust–mantle boundary (e.g., Nicolas 1989; Dick et al. 2006). However, since olivine-rich troctolite was recognized as a possible material from the crust–mantle boundary of a slow-spreading lithosphere, the process of formation of troctolite has been the subject of much discussion (e.g., Drouin et al. 2007, 2009, 2010; Suhr et al. 2008; Renna and Tribuzio 2011; Sanfilippo and Tribuzio 2013a; Sanfilippo et al. 2013).

Most explanations of the formation of olivine-rich rocks have involved reactions between melt and residual peridotite, as represented by the incongruent melting of orthopyroxene to precipitate olivine. Replacive dunite in the residual peridotite, which is commonly observed in the mantle section of ophiolites, indicates that the reaction was caused by reactive porous melt flow in the mantle (e.g., Kelemen et al. 1997). The formation of plagioclase-bearing olivine-rich rocks, such as troctolite, has been explained by reactions related to replacive dunite formation (e.g., Arai and Matsukage 1996; Suhr et al. 2008), and a degree of melt stagnation in the reacting peridotite can produce a variety of olivine-bearing gabbroic rocks (e.g., Arai and Matsukage 1996). The origin of troctolitic rocks can also be explained by fractional crystallization, because the crystallization sequence of a mid-ocean ridge basalt (MORB) melt involves first the crystallization of olivine and then plagioclase (Elthon et al. 1992). These interpretations imply that the products of cumulate processes and reactions should both be considered when discussing the origin of olivine-rich rocks. In spite of their simple mineral assemblages and geochemical features, olivine-rich rocks are heterogeneous on all scales, such as in grain size, volume of plagioclase, and enrichment in incompatible elements (e.g., Arai and Matsukage 1996; Dick and Natland 1996; Suhr et al. 2008). The classification of olivine-rich rocks based on their modal and geochemical compositions hardly discriminates among them. Therefore, understanding the process of their formation is essential when describing olivine-rich rocks from the crust–mantle boundary zone of oceanic lithosphere.

Cumulate rocks in the MORB system have systematic compositional variations controlled by fractional crystallization of the melt. On the other hand, reactions probably also produce olivine-rich rocks with wide ranges of composition, because reaction products are controlled mainly by melt/rock ratios and reactant compositions. The reaction products can be discriminated from the cumulate-origin rocks, based on numerical modeling of the differentiation trend of the melt (e.g., Suhr et al. 2008). Trace-element data of minerals are also helpful to constrain the reaction origin of olivine-rich rocks (e.g., Drouin et al. 2009). However, diversity of the reaction process has not been well examined because of the absence of critical indicators for comparing the reaction products between olivine-rich rock samples. To address the question of how we can discriminate between the reaction processes that form olivine-rich rocks, as well as characterize their petrographical features, we examine trace-element data for spinel-hosted mineral inclusions in olivine-rich rock samples from the ocean floor.

Glass inclusions in spinel have been reported previously from volcanic rocks, and they are useful for investigating primitive melt activity and melting conditions in the mantle because spinel is an excellent container to preserve trapped liquid compositions (Shimizu et al. 2001; Umino et al. 2015). In contrast to these glass inclusions, spinel-hosted mineral inclusions are often observed in olivine-rich rocks as well as in chromitites from the ocean floor and ophiolites, and the inclusions are composed mainly of hydrous silicate minerals such as amphibole and mica that are rich in incompatible elements. Such mineral inclusions have been considered to be the products of melt–peridotite reactions (Arai et al. 1997; Schiano et al. 1997; Arai and Matsukage 1998; Matsukage and Arai 1998; Morishita et al. 2011; Renna and Tribuzio 2011; Sanfilippo and Tribuzio 2013b; Tamura et al. 2014). Tamura et al. (2014) discussed the compositional variations in spinel-hosted pargasite inclusions in terms of the genetic relationships between reacted abyssal peridotite (harzburgite) and olivine-rich troctolite. They suggested that evidence of the reaction sequence had been retained within the spinel-hosted inclusions. Although the mechanisms and dynamics of spinel-armor formation during a reaction remain debated (e.g., Arai and Yurimoto 1994; Zhou et al. 1994), the spinel-trapping stage probably reflects the timing of the reaction process during the formation of the host olivine-rich rock.

The mineral inclusions in spinel have the potential to provide further insights into the histories of formation of rocks that comprise the crust–mantle boundary zone. In this paper, we provide new trace-element compositional data for spinel-hosted pargasite inclusions in olivine-rich rocks from the ocean floor. Taking into account the earlier data of Morishita et al. (2011) and Tamura et al. (2014), we discuss the process of inclusion formation and the significance of the pargasite compositional dataset for understanding the diversity of olivine-rich rocks.

Studied samples from the crust–mantle boundary

We examined spinel-hosted amphibole (pargasite) inclusions in plagioclase-bearing and plagioclase-free olivine-rich rocks, such as troctolite, dunite, and harzburgite. The rock samples were collected over the last 20 years during various expeditions that had examined the crust–mantle section at mid-ocean ridges with fast (EPR: East Pacific Rise), intermediate (CIR: Central Indian Ridge), and slow-spreading rates (MAR: Mid-Atlantic Ridge). Petrographical features and the origin of each sample have already been described in several previous works (see Table 1). The EPR troctolite samples are from an interval in drillcore that was closely related to the harzburgite interval in the Hess Deep rift, EPR (Arai and Matsukage 1996; Dick and Natland 1996). The CIR samples are composed of plagioclase-bearing dunite and troctolite. Along with gabbroic rocks, they were collected during a submersible dive over the

Table 1 Spinel-hosted mineral inclusion bearing samples used in this study

Locality	Sample	Rock type	References
Hess Deep, East Pacific Rise (ODP Leg 147 Hole 895C)	4R-1 72–74 cm	Troctolite	Arai and Matsukage (1996)
	4R-2 97–99 cm	Troctolite	
Uraniwa Hills, Central Indian Ridge	6K925R13	Plagioclase-bearing dunite	Sanfilippo et al. (2015)
	6K925R05	Troctolite	
Atlantis Massif, Mid-Atlantic Ridge (IODP Leg304/305 Site1309)	235R	Olivine-rich troctolite	Tamura et al. (2008, 2014)
	BH1 and BH2	Reacted harzburgite	
Izu-Bonin-Mariana Arc	417R-02	Dunite	Morishita et al. (2011)

Uraniwa Hills, an oceanic core-complex-like hill of ocean floor on the CIR (Morishita et al. 2009; Nakamura et al. 2007; Morishita et al. 2014; Sanfilippo et al. 2015). The MAR troctolite and harzburgite samples are from drillcore intervals of the Atlantis massif on the oceanic core complex at MAR30°N (Tamura et al. 2008, 2014). The MAR troctolites have been described as "olivine-rich troctolites" that formed by multistage reactions between melt and harzburgite (Drouin et al. 2007, 2009, 2010; Suhr et al. 2008). The MAR harzburgite sample was in contact with gabbro and represents the residual peridotite–melt reaction front (Tamura et al. 2008, 2014). We also examined one dunite sample collected along with harzburgite and wehrlite during a submersible dive in the Izu–Bonin–Mariana (IBM) forearc region (Morishita et al. 2011).

The values of Cr# (Cr/[Cr + Al] atomic ratios) for spinels in the samples are largely constant at 0.50–0.58, and the Fo contents of the olivines are also nearly constant at 89–90 (except for a value of 86 in the MAR troctolite). The TiO_2 contents of the spinels are more variable (up to 2 wt%), and low (0.1–0.4 wt%) in plagioclase-free samples. The anorthite contents of plagioclases in the EPR and MAR troctolites are 81–85 and 76, respectively. Sample localities and mineral chemistries are summarized in Tables 1 and 2, respectively.

Petrography and geochemistry of the pargasite inclusions

Subhedral to anhedral spinel grains contain single or multiple inclusions of either single or multiple minerals. The inclusions are round to angular in shape, and range in diameter from 10 to 100 μm. Pargasite is the dominant phase in these spinel-hosted inclusions (Fig. 1a, b), and in the cases of multi-mineral inclusions, aspidolite (Na-phlogopite) and/or pyroxenes coexist with the pargasite (Fig. 1c, d). Irregularly shaped orthopyroxene is commonly observed with pargasite in the spinel-hosted inclusions of the mid-ocean ridge samples. The morphological relationships between the pargasite and other mineral grains are often not clearly observable in thin section, but orthopyroxene has been observed enclosed by pargasite (Fig. 1c, e, f). Orthopyroxene inclusions are present but rare in the spinels of the reacted MAR harzburgite (Tamura et al. 2014), and paired inclusions of pargasite and clinopyroxene are characteristic of the IBM dunite sample (Morishita et al. 2011).

Major-element and trace-element compositions of amphibole inclusions in spinel and the host rock minerals were determined using an electron microprobe (JEOL-JXA8800) and laser ablation ICP–MS (Microlas GeoLas Q-plus and Agilent 7500 s) at Kanazawa University, Japan (Morishita et al. 2005). Details of the analytical conditions and data reduction methods are given in Tamura et al. (2014). Compositions of amphibole inclusions are listed in Table 3.

The amphibole inclusions have pargasitic compositions with TiO_2 contents up to 5.6 wt%. The pargasite inclusions in the plagioclase-free samples (MAR harzburgite and IBM dunite) have low values of TiO_2 (1–2 and <0.6 wt%, respectively), whereas inclusions in the plagioclase-bearing samples have high values (Fig. 2). The incompatible-trace-element compositions of the pargasite inclusions are highly variable between samples, and they display flat, LREE-enriched or M-shaped rare earth element (REE) patterns (Fig. 3). Pargasite inclusions in the EPR troctolite and CIR dunite samples have high REE abundances (10–100 times chondrite), whereas abundances are low in the CIR troctolite inclusions. Their trace-element patterns characteristically show strong negative Eu and Sr anomalies, but no anomalies are seen in the REE patterns of the MAR and IBM samples (Fig. 4). The pargasite inclusions in the IBM dunite have lower REE abundances (1–4 times chondrite) than those in the mid-ocean ridge samples (Fig. 3). The trace-element patterns of most pargasite inclusions show positive anomalies for the high-field-strength elements (HFSEs: Nb, Ta, Zr, Hf, and Ti) relative to the neighboring REEs, while four out of five sets of data for the EPR samples show a negative Ti anomaly or no anomaly at all (Fig. 4). As shown in Fig. 5, the samples are distinguished by their characteristic Eu and Zr anomalies.

Table 2 Averaged compositions of olivine, spinel, plagioclase and clinopyroxene in studied samples

	EPR (895C)				CIR (6K925)				IBM	
	4R-1		4R-2		R05		R13		417R-02	
	Troctolite		Troctolite		Troctolite		Plg-Dunite		Dunite	
Olivine		$n = 3$		$n = 4$		$n = 6$		$n = 7$		
Fo	89.2	(0.4)	89.8	(0.6)	88.7	(0.5)	89.9	(0.5)	na	
NiO (wt%)	0.30	(0.02)	0.28	(0.02)	0.28	(0.09)	0.32	(0.07)	na	
Spinel		$n = 5$		$n = 5$		$n = 5$		$n = 13$		$n = 51$
Mg#	0.529	(0.119)	0.559	(0.106)	0.512	(0.068)	0.569	(0.036)	0.590	(0.059)
Cr#	0.549	(0.054)	0.541	(0.056)	0.521	(0.096)	0.576	(0.040)	0.535	(0.027)
TiO_2 (wt%)	1.1	(0.48)	0.89	(0.27)	0.85	(0.41)	2.01	(0.34)	0.13	(0.06)
Plagioclase		$n = 3$		$n = 4$						
An	84.6	(0.1)	81.6	(0.1)	na		na		–	
Clinopyroxene		$n = 3$		$n = 3$	na			$n = 2$	Inc[b]	$n = 11$
SiO_2 (wt%)	52.49	(1.09)	52.65	(0.00)			52.90	(0.21)	54.14	(1.28)
TiO_2	0.45	(0.01)	0.50	(0.12)			0.93	(0.08)	0.10	(0.09)
Al_2O_3	3.05	(0.29)	3.21	(0.28)			2.70	(0.19)	2.11	(1.92)
Cr_2O_3	1.28	(0.26)	1.21	(0.07)			1.11	(0.09)	1.15	(0.65)
FeO[a]	3.08	(0.50)	3.06	(0.27)			2.59	(0.01)	2.08	(1.32)
MnO	0.10	(0.04)	0.10	(0.04)			0.11	(0.06)	0.05	(0.07)
MgO	17.09	(1.23)	16.89	(0.12)			17.05	(0.36)	16.46	(1.49)
CaO	22.56	(1.73)	22.77	(0.70)			21.78	(0.07)	23.14	(2.63)
Na_2O	0.43	(0.09)	0.48	(0.04)			0.69	(0.11)	0.95	(0.85)
NiO	0.04	(0.02)	0.02	(0.05)			0.04	(0.03)	0.02	(0.05)
Total	100.56		100.88				99.90		100.22	
Mg#	0.908	(0.009)	0.908	(0.007)			0.921	(0.002)	0.934	(0.042)
								$n = 6$		$n = 7$
Ti (μg/g)	2579	(148)	2817	(918)			4576	(1225)	712	(546)
Sr	5.8	(1.2)	7.4	(3.0)			6.7	(1.13)	18.3	(5.8)
Y	32.2	(1.1)	19.4	(5.4)			36.5	(10.3)	9.5	(2.8)
Zr	28.2	(4.1)	13.6	(9.1)			37.8	(21.6)	14.5	(8.9)
Nb	0.22	(0.11)	0.28	(0.01)			0.21	(0.10)	0.20	(0.17)
La	0.30	(0.04)	0.19	(0.03)			0.61	(0.41)	0.34	(0.28)
Ce	2.03	(0.18)	1.26	(0.15)			3.92	(2.46)	2.22	(1.50)
Pr	0.51	(0.07)	0.31	(0.10)			0.90	(0.50)	nd	
Nd	3.73	(0.41)	2.19	(0.86)			6.22	(3.10)	1.90	(0.48)
Sm	2.23	(0.13)	1.21	(0.56)			3.16	(1.24)	0.61	(0.17)
Eu	0.44	(0.05)	0.47	(0.30)			0.72	(0.20)	0.25	(0.09)
Gd	3.94	(0.09)	2.17	(0.94)			5.06	(1.79)	0.96	(0.27)
Tb	0.78	(0.03)	0.44	(0.16)			0.94	(0.33)	nd	
Dy	6.08	(0.16)	3.44	(1.11)			6.99	(2.18)	1.53	(0.56)
Ho	1.30	(0.10)	0.74	(0.21)			1.44	(0.43)	nd	
Er	3.62	(0.02)	2.19	(0.50)			3.93	(1.00)	1.15	(0.43)
Tm	0.49	(0.03)	0.32	(0.05)			0.53	(0.12)	nd	
Yb	3.05	(0.19)	2.02	(0.44)			3.15	(0.55)	1.04	(0.38)
Lu	0.37	(0.04)	0.28	(0.07)			0.39	(0.08)	0.13	(0.04)
Hf	1.00	(0.16)	0.46	(0.41)			1.15	(0.73)	0.74	(0.38)

Mg# = Mg/(Mg + Fe); Cr# = Cr/(Cr + Al)

For MAR sample data, see Tamura et al. (2014)

n number of analyses, 2 standard deviation in parentheses, *na* not analyzed because of alteration, *nd* not determined

[a] Total iron as FeO

[b] Clinopyroxene data of IBM dunite is from inclusions in spinel

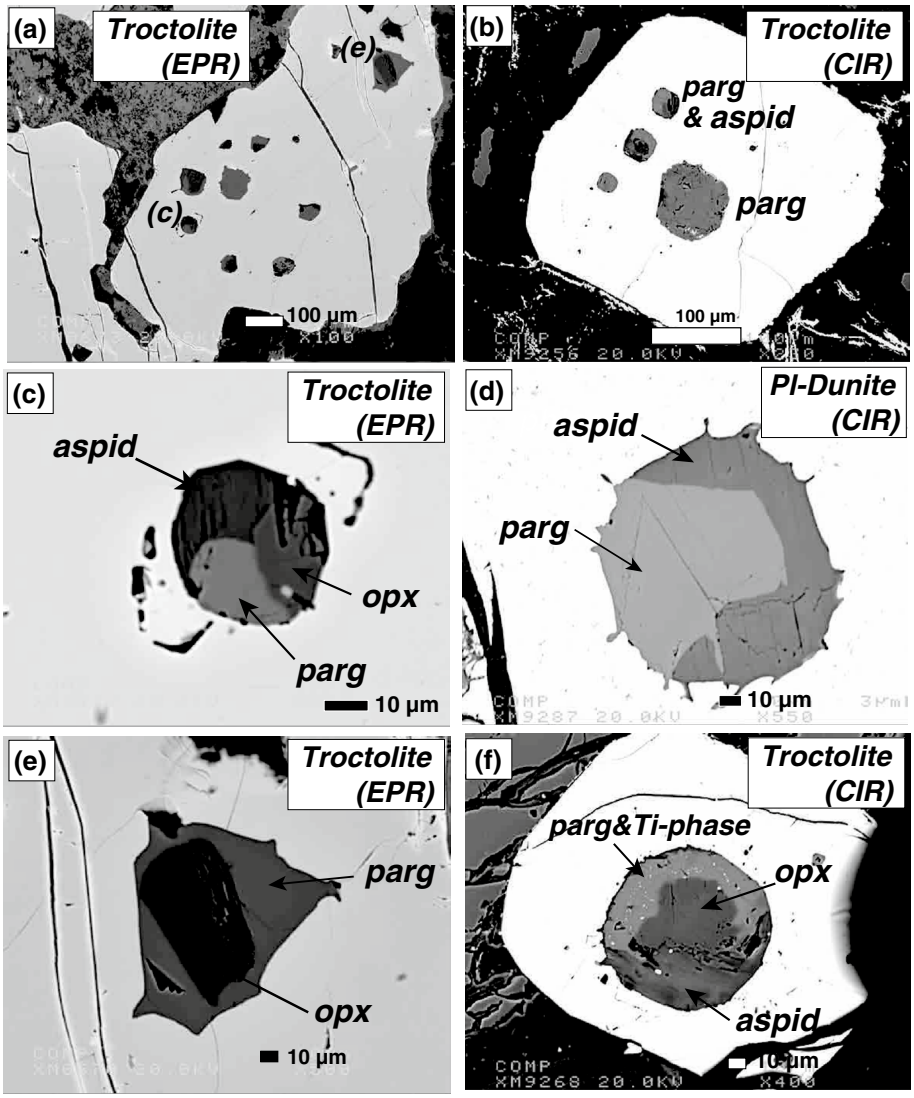

Fig. 1 Back-scattered electron images of spinel-hosted mineral inclusions in the studied samples from the EPR and CIR. **a**, **b** Multiple inclusions in spinel sometimes composed just of pargasite or sometimes poly-mineral phases (pargasite and aspidolite). **c**–**f** Poly-mineral inclusions: pargasite–orthopyroxene–aspidolite, pargasite–aspidolite, and pargasite–orthopyroxene. The inclusions of (**c**) and (**e**) coexisted, as shown in (**a**). Ti–rich particles (*white spots*) are observed in the pargasite (*lighter part*) in (**f**). Note that orthopyroxene commonly coexists with pargasite, but in the IBM dunite the pargasite–clinopyroxene pair has been observed (see Morishita et al. 2011)

Discussion

Hydrous mineral inclusions in spinel and their origin

Hydrous silicate minerals, such as pargasite and aspidolite, which are characteristically rich in incompatible elements (e.g., Na, H_2O, HFSEs, and REEs), have often been reported as spinel-hosted inclusions in troctolite, dunite, and reacted harzburgite as well as in chromitite (e.g., Arai et al. 1997; Tamura et al. 2008, 2014; Renna and Tribuzio 2011). Tamura et al. (2008, 2014) reported spinel-hosted pargasite inclusions from a reacted harzburgite and suggested that they are the products of reaction between melt and residual peridotite. On the other hand, many olivine-rich rock samples are not equivalent to a residual peridotite (such as a harzburgite), although the chemical compositions of their minerals may indicate a reacted peridotite origin rather than a cumulate origin (e.g., Arai et al. 1997; Suhr et al. 2008; Sanfilippo et al. 2015). Here, as a first approach, we discuss the formation of spinel-hosted hydrous minerals in the context of the origin of the olivine-rich rock: was it a cumulate from a MORB melt or a reacted mantle peridotite?

Pargasite and aspidolite are exceptionally found as the spinel-hosted inclusions in all our studied samples. Fractionation of a MORB melt can primarily form olivine-rich gabbroic rocks, including troctolite, because the first mineral to crystallize is olivine, followed by plagioclase and clinopyroxene (e.g., Elthon et al. 1992; Grove et al. 1992). On the other hand, hydrous minerals are commonly observed in evolved gabbroic rocks from the ocean floor, and the formation of an amphibole-bearing gabbroic rock, for example, requires the presence of an evolved hydrous silicate melt or water–rock reactions (e.g., Coogan et al. 2001; Gillis and Mayer 2001). In contrast to olivine-rich rocks, amphibole-bearing gabbros rarely contain spinel,

Table 3 Major- and trace-element compositions of spinel-hosted amphibole inclusions

	EPR					CIR						IBM	
	895C4R-1 Troctolite			895C4R-2 Troctolite		6K925-R13 Plag-Dunite					6K925-R05 Troctolite	417R-02 Dunite	
	S301	S302	S303	S001	S101	102	202	203	301-2	501-2	101-2	spx109	spx111
SiO_2 (wt%)	43.90	44.13	44.29	44.05	44.94	42.47	43.39	43.13	43.18	43.60	46.76	48.42	46.56
TiO_2	3.32	3.26	3.97	3.10	2.78	5.64	4.90	5.08	5.14	4.05	2.24	0.23	0.28
Al_2O_3	11.23	11.53	11.22	11.72	11.23	11.04	10.72	11.13	10.93	10.87	10.00	9.81	10.60
Cr_2O_3	2.24	2.23	2.04	2.04	2.02	2.14	2.05	2.03	2.37	2.29	1.69	1.87	2.38
FeO	4.20	4.13	4.19	3.45	3.58	4.24	3.99	4.01	3.74	4.08	4.06	2.06	2.88
MnO	0.09	0.09	0.10	0.03	0.07	0.09	0.08	0.09	0.07	0.06	0.10	0.03	0.04
MgO	17.71	17.90	17.65	18.39	18.90	16.13	16.57	16.78	17.22	16.79	18.98	20.81	19.77
CaO	10.77	10.85	11.49	11.96	10.92	10.78	11.44	11.34	11.01	11.66	12.35	11.31	11.22
Na_2O	3.97	4.06	3.85	3.67	3.73	4.30	3.85	4.14	4.16	4.24	2.35	4.24	4.38
K_2O	0.03	0.06	0.05	0.07	0.03	0.01	0.05	0.01	0.02	0.02	0.03	0.00	0.02
NiO	0.07	0.08	0.07	0.08	0.09	0.10	0.08	0.10	0.08	0.09	0.02	0.04	0.06
Total	97.51	98.31	98.91	98.54	98.29	96.94	97.12	97.84	97.91	97.74	98.56	98.82	98.20
Mg#	0.883	0.885	0.883	0.905	0.904	0.871	0.881	0.882	0.891	0.880	0.893	0.947	0.924
LA	30/5	30/5	30/5	20/5	30/5	30/5	20/5	20/5	20/5	20/5	20/5	20/5	20/5
Ti (μg/g)	20,498	18,838	24,916	19,628	18,246	40,612	31,417	33,600	31,336	25,932	14,008	1947	2606
Cr	16,120	13,101	16,621	12,341	11,435	16,701	14,411	14,425	14,075	16,977	8632	15,804	14,631
Sr	85.29	67.54	86.92	108.21	75.24	101.71	71.80	63.04	75.46	97.82	46.61	16.22	52.14
Y	88.58	66.07	73.74	93.28	126.97	94.12	112.05	46.77	52.80	60.09	21.53	6.32	6.13
Zr	418	388	511	265	683	1042	788	769	741	1105	66.8	31.87	48.10
Nb	34.63	28.13	71.23	11.57	23.58	86.04	114.15	68.78	24.65	3.60	3.51	10.04	29.57
Ba	2.59	4.31	2.92	2.63	1.40	1.10	3.04	1.13	1.12	1.20	1.02	<0.64	<0.64
La	1.91	1.51	3.56	2.72	2.31	6.32	6.50	5.67	8.67	6.62	0.80	0.27	0.52
Ce	11.30	8.02	28.13	13.88	15.68	73.19	51.79	45.23	53.34	37.35	6.55	1.30	1.99
Nd	21.64	14.50	26.41	16.52	21.30	68.47	52.89	49.98	31.04	17.94	9.36	1.30	1.83
Sm	10.40	7.21	7.17	7.32	10.73	11.77	13.10	11.73	7.43	3.09	2.42	<0.50	0.39
Eu	1.52	1.18	1.23	0.74	1.28	2.43	1.89	1.82	1.44	0.69	0.37	0.23	0.15
Gd	13.95	9.78	7.77	12.46	17.46	10.72	14.80	9.70	7.65	3.16	2.04	0.59	0.52
Dy	16.36	11.90	11.37	18.87	24.10	13.64	18.96	7.43	9.08	8.95	3.25	1.04	1.07
Er	8.86	7.09	10.51	10.21	10.14	10.56	11.73	4.29	5.14	9.10	2.30	0.76	0.82
Yb	6.46	5.80	11.12	7.69	7.33	10.54	8.57	3.51	4.51	8.77	3.13	0.65	0.81
Lu	0.78	0.71	1.36	0.86	0.85	1.28	0.93	0.37	0.51	1.00	0.47	<0.11	<0.11
Hf	12.71	10.95	15.89	8.08	16.55	33.06	27.01	28.65	26.60	26.06	3.15	0.95	1.43
Ta	1.81	1.31	4.10	0.94	1.12	6.09	6.79	4.93	1.94	0.21	0.39	0.43	1.52

Total iron as FeO

Mg# = Mg/(Mg + Fe) atomic ratio

For MAR and IBM sample data, see Tamura et al. (2014) and Morishita et al. (2011)

LA laser ablation condition for laserspot diameter (μm)/repetition rate (Hz)

because spinel is a mineral that develops from less-evolved basaltic melts (e.g., Roeder and Reynolds 1991; Barns and Roeder 2001). It is unlikely, therefore, that the spinels would have included amphibole grains during fractional crystallization. Similarly, one would not expect an evolved hydrous melt to be trapped during the crystallization of spinel.

Several researchers have already shown that olivine-rich rocks can be produced by reactions between melt and mantle peridotite (e.g., Arai and Matsukage 1996;

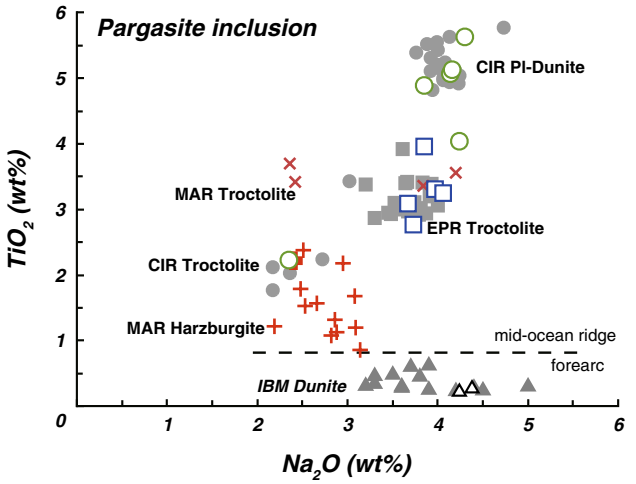

Fig. 2 Na_2O–TiO_2 compositional relationships in pargasite inclusions in the olivine-rich rocks. *Open symbols* are pargasite inclusions with trace-element data discussed in this study. *Gray closed symbols* show other pargasite inclusions in each sample. MAR samples and IBM dunite data are from Tamura et al. (2014) and Morishita et al. (2011), respectively

Suhr et al. 2008; Dick et al. 2010), and based on our previous study (Tamura et al. 2014), we propose here that the spinel-hosted hydrous minerals provide evidence that the studied olivine-rich rocks are the products of reactions involving mantle peridotite. This proposition is supported by the likelihood that simple fractionation of a MORB melt could not have produced spinels with such inclusions.

Arai et al. (1997) and Schiano et al. (1997) described spinel-hosted hydrous mineral inclusions in olivine-rich rocks from the ocean floor and from ophiolites, and they suggested that the inclusions were formed from melts that had been trapped in the spinels. To explain the formation of hydrous silicate minerals within the spinel, Arai et al. (1997) suggested that the trapped melt had formed by reactions between an olivine-saturated melt and a residual peridotite (such as lherzolite or harzburgite) and that the process involved the incongruent melting of orthopyroxene to precipitate olivine. The compositions of this secondary melt were not only selectively enriched in SiO_2 and incompatible elements including H_2O, but also in Cr due to olivine precipitation. If such a SiO_2-rich melt were mixed with an olivine-saturated melt, the precipitation of spinel would have been enhanced (Arai and Yurimoto 1994; Arai and Matsukage 1998; Arai and Miura 2015).

The reaction between a melt and a residual peridotite, as stated above, primarily corresponds to the formation of a replacive dunite, which is commonly observed in the mantle section of ophiolites (e.g., Kelemen et al. 1997; Akizawa et al. submitted). These replacive dunites are formed from residual peridotites by porous melt flow in the mantle (e.g., Kelemen et al. 1995). Primitive MORB melts are produced by partial melting of source mantle beneath a mid-ocean ridge, and they eventually produce a basaltic oceanic crust (e.g., Grove et al. 1992). Such primitive MORB melts are reactive to residual peridotites (especially their orthopyroxenes) during melt extraction and transportation, because the melts were formed at high pressure and are then in disequilibrium with mantle peridotites under lower-pressure conditions (e.g., Kelemen et al. 1995; Arai and Matsukage 1996). We suggest, therefore, that the spinel-hosted hydrous minerals would be expected to form when replacive dunite is formed in the mantle.

As an analog of the reaction product between a melt and a residual peridotite, Arai and Abe (1995) described olivine–clinopyroxene–spinel–glass aggregates along the boundaries between orthopyroxenes in mantle xenoliths and the host alkali basalt melt. Su et al. (2012) indicated that olivine, amphibole, feldspar, and glass (rich in SiO_2 and alkalis) in mantle xenoliths were formed from secondary melts generated by reactions in the mantle between the orthopyroxene and the host magma. Experimental studies by Shaw et al. (1998) and Shaw (1999) demonstrated that SiO_2 and alkali elements were preferentially concentrated along the reaction zone between orthopyroxenes and alkali basalt melt and that the reaction consequently enhanced the extensive crystallization of olivine. Although we are unable to constrain the melt-entrapment dynamics during spinel crystallization, these previous studies support the idea that the orthopyroxene decomposition reaction has a high potential for simultaneously producing enrichments of incompatible elements in the melt and during the crystallization of spinel.

Numerical modeling of residual peridotite compositions indicates that fractional melting takes place during melt extraction from the mantle beneath a mid-ocean ridge. Thus, the incompatible-element compositions of partial melts from the source mantle are not consistent with those of MORB (Johnson et al. 1990). This type of melting regime suggests that a fraction of enriched melt, such as alkali basalt, can be produced and then undergo reaction with the residual peridotite. Hence, the analogs of the reaction process discussed above are likely to occur, even beneath a mid-ocean ridge. Spinel grains with hydrous mineral inclusions are rarely observed in residual peridotites such as lherzolite and harzburgite, and this is consistent with the proposal that reaction processes (that form replacive dunite) are necessary for the formation of the mineral inclusions beneath a mid-ocean ridge, rather than partial melting processes.

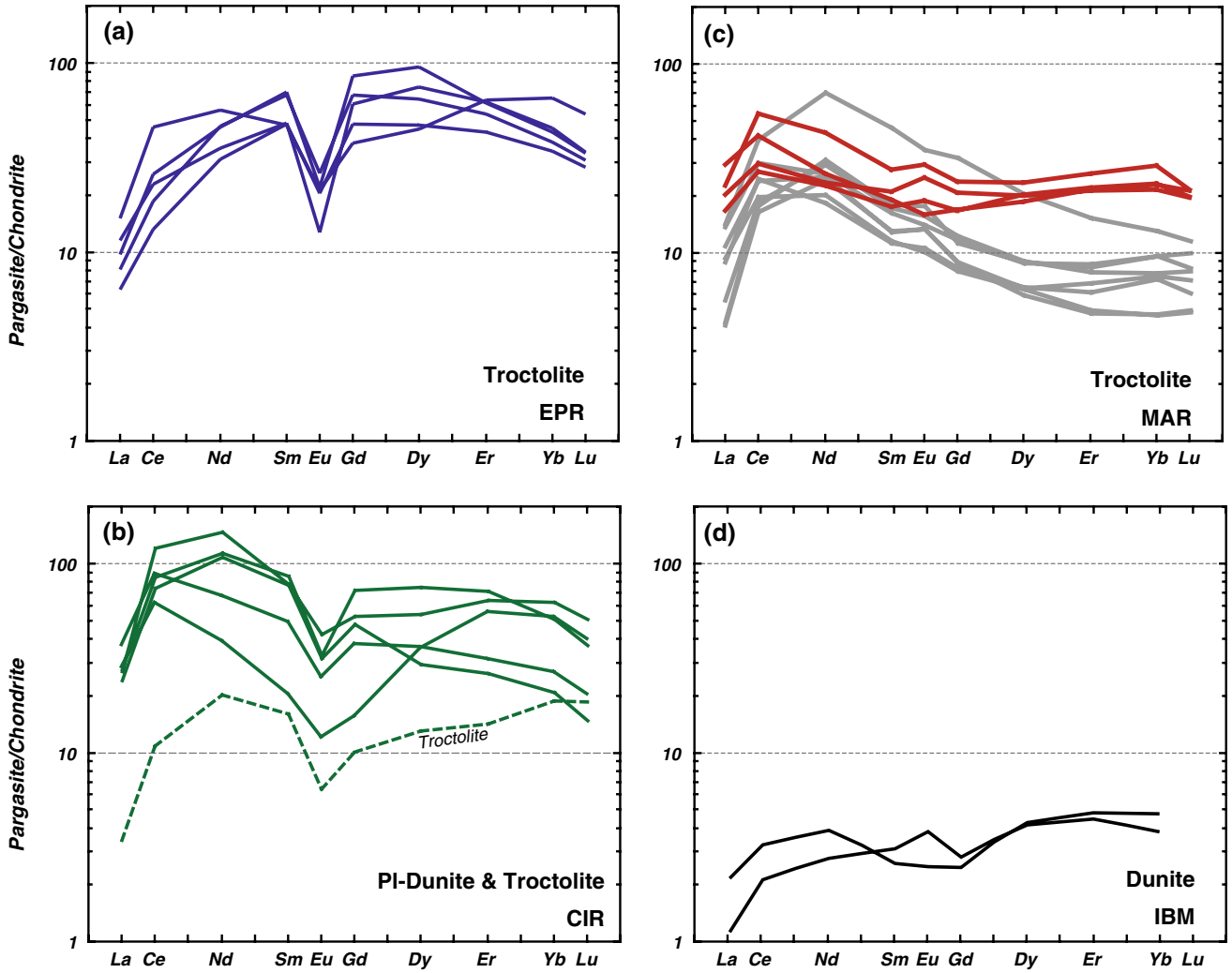

Fig. 3 Rare earth element patterns of pargasite inclusions in the studied samples. MAR samples (*gray lines* harzburgite) and IBM dunite data are from Tamura et al. (2014) and Morishita et al. (2011), respectively. Chondrite values are from Sun and McDonough (1989)

Interpretation of pargasite geochemistry and the formation of olivine-rich rocks

The reactions that form replacive dunite from residual peridotite are expected to involve the formation of olivine-rich rocks along mid-ocean ridges (Arai and Matsukage 1996; Suhr et al. 2008; Dick et al. 2010). Here, we discuss the variations in trace-element compositions of spinel-hosted pargasite inclusions in order to discriminate and constrain the conditions of the reaction processes that form olivine-rich rocks along the crust–mantle boundary of the oceanic lithosphere.

In each of our studied sample, the incompatible-trace-element compositions of the pargasite inclusions are very similar, even though the coexisting inclusion minerals are variable. The incompatible-element partitioning between pargasite inclusions and the host rock clinopyroxene is relatively constant in the mid-ocean ridge samples (Fig. 6), whereas the trace-element compositions of the pargasite vary among samples (Figs. 2, 3, 4). However, the element partitioning is distinct from the typical partitioning for coexisting amphibole–clinopyroxene pairs in gabbros and peridotites (Fig. 6). This indicates that the pargasite inclusions did not crystallize from an evolved melt in equilibrium with the host rock clinopyroxene. This evidence of disequilibrium probably supports the proposals given above for the origin of inclusions, with the pargasite inclusions in the studied samples being formed by reaction. Assuming that the spinel crystallization in the reaction (when melt or minerals were trapped in spinel) occurred during the initial formation of the host olivine-rich rock, the differences in pargasite inclusion compositions reflect the diversity of the reactions in the rock-forming history.

The REE patterns of pargasite inclusions in the EPR and CIR samples characteristically show negative Eu anomalies (Fig. 3). This implies that the pargasite was

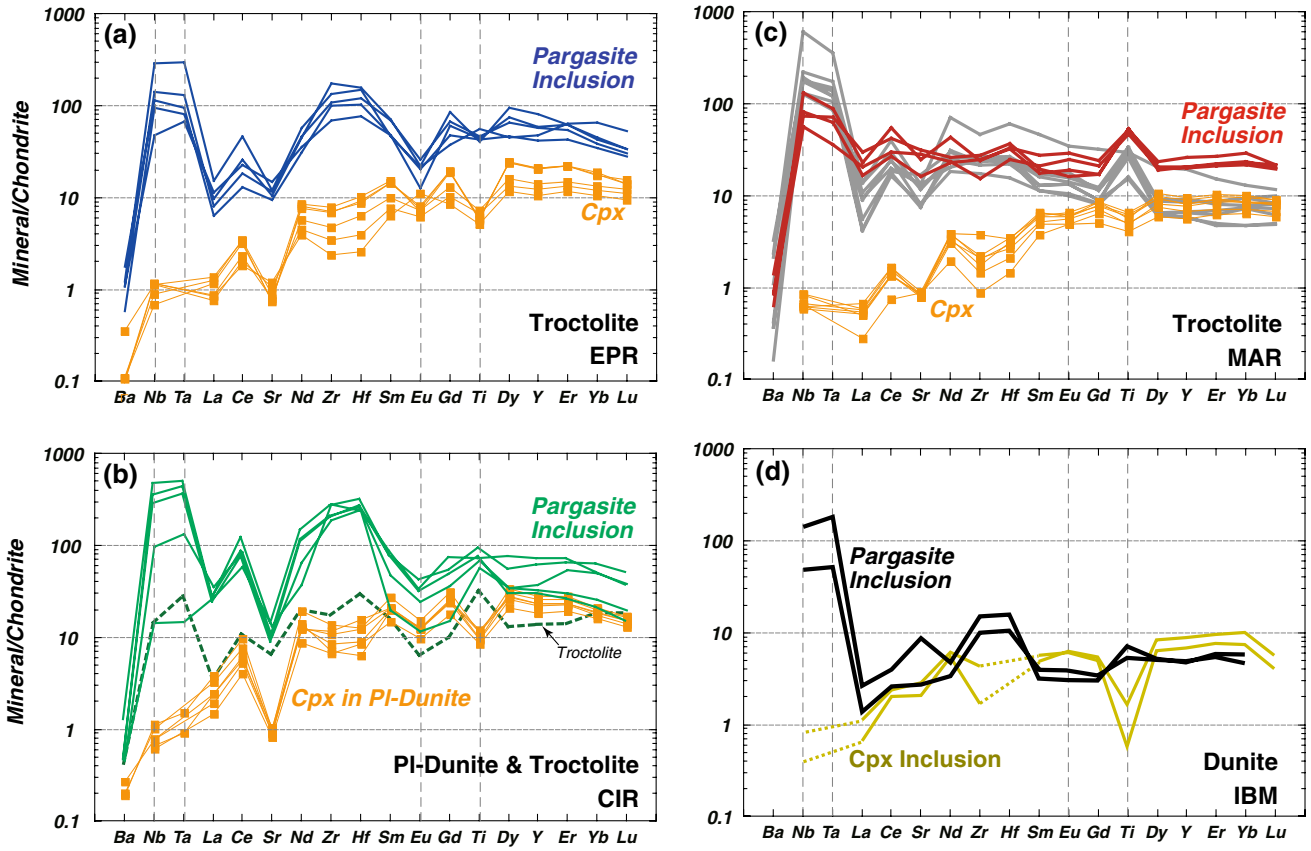

Fig. 4 Incompatible-trace-element patterns of pargasite inclusions in the studied samples. MAR samples (*gray lines* harzburgite) and IBM dunite data are from Tamura et al. (2014) and Morishita et al. (2011), respectively. Compositions of host rock clinopyroxenes are shown for comparison. No clinopyroxene data are available for the CIR troctolite in (**b**). Spinel-hosted clinopyroxene inclusion data for the IBM dunite are given in (**d**). Chondrite values are from Sun and McDonough (1989)

crystallized from an evolved melt that had already fractionated plagioclase. As shown in Fig. 5a, in terms of the values of Eu/Eu* (= $Eu_{CN}/[Sm_{CN}*Gd_{CN}]^{1/2}$; CN: chondrite normalized value) and Zr/Zr* (= $Zr_{CN}/[Nd_{CN}*Sm_{CN}]^{1/2}$) in the pargasite inclusions, the EPR and CIR samples can be clearly discriminated from the MAR samples. Therefore, these compositional features should be useful in deciphering the origin of the pargasite inclusions. Here, we tentatively consider a melt that is crystallizing pargasite with Eu and Zr anomalies based on the partition coefficients between pargasite and melt, which do not cause the fractionation of Zr and Eu (i.e., $D_{Zr/Zr^*} \leq 1$, $D_{Eu/Eu^*} \geq 1$; Ozawa and Shimizu 1995). The Eu and Zr anomalies in the pargasites of the EPR and CIR samples are unlikely to be explained by the compositions of the secondary melt produced by the reaction involving orthopyroxene decomposition. Orthopyroxene in the residual harzburgite is a better host for Zr relative to Nd and Sm (Fig. 5b), as indicated by the partition coefficient $D_{Zr/Zr^*} = 4.95$ (Ozawa and Shimizu 1995), and the incongruent melting of orthopyroxene possibly creates the high-Zr/Zr* secondary melt. However, crystallization of the host spinel and olivine, as well as mixing with the primitive melt, should be taken into account because of the high compatibility of Zr in spinel ($D_{Zr/Zr^*} \geq 100$) and the fact that the pargasite in the MAR samples shows no significant enrichment in Zr (Fig. 5a). In either case, the secondary melt itself could not have caused the low values of Eu/Eu* in the pargasites because the specific fractionation of Eu is unrealistic during the precipitation of olivine and spinel. Hence, the reactant melt composition is most probably responsible for the Eu and Zr anomalies in the pargasite inclusions.

In the numerical model, the Eu/Eu* values of the pargasite inclusions in EPR and CIR samples can be attained by 30–85 % fractionation of plagioclase from the MORB melt. The Eu/Eu* values of the calculated melt in equilibrium with the host rock clinopyroxene are equivalent to those of the pargasite inclusions (Fig. 5). The fact that the values of Zr/Zr* and Eu/Eu* in the calculated melt can be reproduced by the fractional crystallization of plagioclase and clinopyroxene after olivine suggests that such an

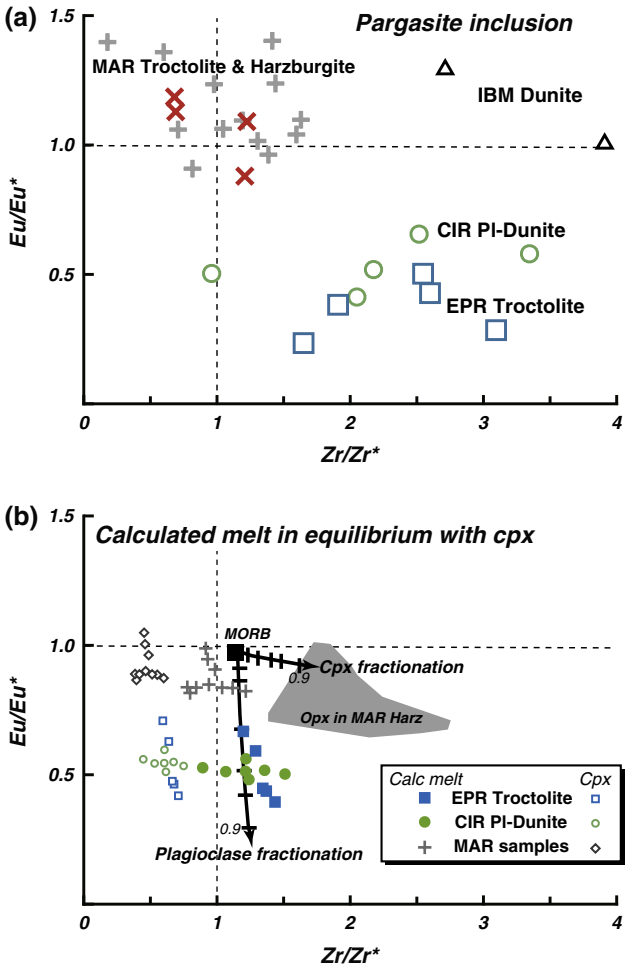

Fig. 5 **a** Compositional relationships between Eu/Eu* and Zr/Zr* values of pargasite inclusions in the studied samples. MAR samples (×, troctolite; +, harzburgite) and IBM dunite data are from Tamura et al. (2014) and Morishita et al. (2011), respectively. Note that pargasite coexists with clinopyroxene, as spinel-hosted inclusions, in the IBM dunite (see text). $Eu/Eu^* = Eu_{CN}/(Sm_{CN}{}^*Gd_{CN})^{1/2}$; $Zr/Zr^* = Zr_{CN}/(Nd_{CN}{}^*Sm_{CN})^{1/2}$; *CN* chondrite normalized value (Sun and McDonough 1989). **b** Compositions of the calculated melt in equilibrium with host rock clinopyroxene in the studied samples. Partition coefficients used for the calculations were selected from Ozawa and Shimizu (1995) and Gurenko and Chaussidon (1995). *Arrows* indicate tentative compositional trends of MORB melt during fractional crystallization of plagioclase and clinopyroxene, respectively. *Ticks* indicate crystal fraction ($F = 0.1$, 0.2, 0.3, 0.5, 0.8, and 0.9). The MORB melt composition is from Reynolds and Langmuir (1997). *Gray field* shows the composition of orthopyroxenes that coexist with spinel with mineral inclusions in the MAR harzburgite (Tamura et al. 2008)

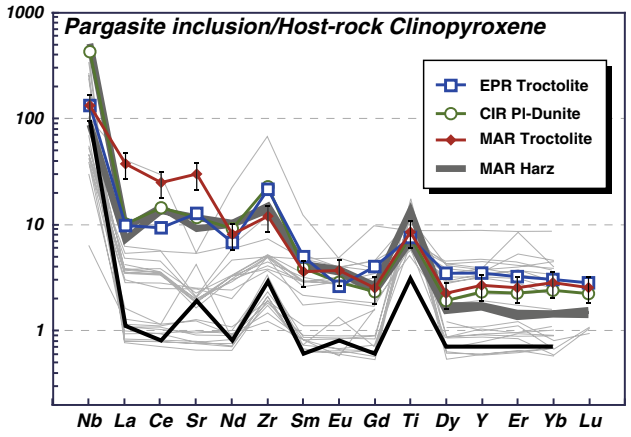

Fig. 6 Trace-element partitioning between spinel-hosted pargasite inclusions and the host rock clinopyroxene. Averaged concentrations were used. An *error bar* of 30 % is shown with the data for the MAR troctolite. The *black line* shows the partitioning between the pargasite and clinopyroxene inclusions in the IBM dunite (see text). The *thin gray lines* show the partitioning of coexisting amphibole–clinopyroxene pairs in peridotites and gabbros (compiled by Tamura et al. 2014)

evolved melt was available during the period of rock formation. However, it is difficult to reproduce the high values of Zr/Zr* in the pargasite inclusions by simple fractionation of plagioclase and clinopyroxene from the MORB melt, but they could be produced by further differentiation of the secondary melt (Fig. 5b). Here, we expect that the secondary melt coexisted and reacted with the evolved melt, although the nature of any elemental exchange between those two melts is uncertain. Coogan et al. (2000) suggested that the extensive Zr enrichment in the clinopyroxenes of gabbroic rocks could be accomplished by mixing of a highly evolved melt, such as an interstitial melt, with the melt flowing through the crystal mush. A similar mixing mechanism may be locally responsible for the reaction that produced the high values of Zr/Zr* in the pargasites of the EPR and CIR samples. Accordingly, the formation of spinels with mineral inclusions in the EPR and CIR samples probably involved the crystallization of plagioclase and clinopyroxene from evolved melts in the host rock.

Based on the compositional differences in the pargasite inclusions of the EPR and CIR samples versus those in the MAR troctolite, we can now discuss the history of the conversion of mantle peridotites to olivine-rich rocks. Beneath a mid-ocean ridge, the migration of partial melts in the mantle results in the formation of replacive dunites in residual peridotites; however, most of the partial melt accumulates as a MORB melt that eventually forms the oceanic crust (Johnson et al. 1990; Grove et al. 1992; Kelemen et al. 1995). Therefore, it can be expected that MORB melts coexist with reacted mantle rocks, which eventually form the crust–mantle boundary zone. An example is the dunite or gabbroic rock coexisting with harzburgite, as observed at the top of the mantle section in the Oman ophiolite (e.g., Akizawa et al. 2012). The compositions of pargasite inclusions in the EPR and CIR samples probably reflect the contributions of the evolved melt to the reaction. For the formation of the EPR and CIR samples, we suppose that the reaction

between melt and residual peridotite (i.e., spinel crystallization) occurred at a site where plagioclase-fractionated melts were produced at the same time. To account for the coexistence of secondary and evolved melts, reactions between melt and residual peridotite in the melt-focusing zone, perhaps in the presence of high melt/rock ratios, seem reasonable, as the initiation of crystallization from a MORB melt can be assumed to take place in a zone of focused melt flow rather than in a zone of porous melt flow in the mantle.

The trace-element patterns of the pargasite inclusions in the MAR harzburgite and MAR troctolite are slightly different (Fig. 4c). Pargasite inclusions in both samples are characterized by the absence of negative Eu anomalies and the presence of weak positive Zr anomalies (Figs. 3, 5). The compositional features indicate that the formation of spinel-hosted pargasite was not affected by an evolved MORB melt. Suhr et al. (2008) reported that the MAR troctolite was finally formed by the crystallization of plagioclase and clinopyroxene from a pervasive MORB-like melt in the replacive dunite. Tamura et al. (2014) suggested that the inclusions provide evidence that the MAR troctolite was formed by the conversion of a residual harzburgite via replacive dunite. The spinel grains with hydrous mineral inclusions in the MAR troctolite had already started to form during the formation of the replacive dunite from the residual peridotite, or at least prior to the crystallization of plagioclase in the troctolite sample. During the formation of replacive dunite, the melt should only rarely have stagnated and been differentiated during porous flow and extraction of the partial melt from the upper mantle, and this would have been in contrast to the situation with focused melt flow.

The trace-element compositions of spinel-hosted pargasite inclusions probably reflect the differences in the melt flow style during the reaction, such as the initiation of olivine-rich rock formation. Determination of the timing and condition of inclusion formation (i.e., initiation of spinel crystallization) would be helpful in characterizing the formation histories of the olivine-rich rocks that comprise the crust–mantle boundary zone where residual peridotite and melt coexisted.

Inheritance from mantle peridotite

The secondary melts contributing to the formation of spinels and their inclusions were generated by a combination of orthopyroxene decomposition and olivine crystallization in the residual peridotite. The compositions of inclusion minerals depend mainly on the compositions of the reactants; i.e., the residual peridotite and the melt. Therefore, the variations in pargasite compositions should partly reflect the residual peridotite compositions, which are controlled mainly by the degree of partial melting.

The incompatible-trace-element abundances in pargasite inclusions in spinels of the IBM dunite are clearly low relative to those of pargasites in mid-ocean ridge samples (Figs. 2, 3). Because no plagioclase grains were observed in either the IBM dunite or the MAR harzburgite, interference from an evolved melt can be ignored in the formation of the inclusions. The incompatible-element compositions of residual peridotite, especially the HREE abundances, are controlled primarily by the degree of melting (e.g., Hellebrand et al. 2001). The HREE abundances of pargasites in the IBM dunite (Yb = 0.65–0.81 ppm) are lower than those in the MAR harzburgite (Yb = 0.79–1.62 ppm) (Fig. 3), indicating that the precursor residual peridotite that was involved in the formation of the IBM dunite was rather depleted. This inference is consistent with the fact that residual peridotites from a forearc region, such as the IBM region, are more depleted than those from a mid-ocean ridge (e.g., Parkinson and Pearce 1998; Tamura and Arai 2006), although the Cr# values in spinels, which also provide an indication of the degree of partial melting (e.g., Arai 1994; Hellebrand et al. 2001), are not critically different between the studied samples (Cr# = 0.52–0.57; Table 2). With regard to other spinel-hosted inclusion minerals, clinopyroxene coexists with pargasite in the IBM dunite whereas orthopyroxene is commonly observed in the mid-ocean ridge samples. The compositional relationships between pargasite and clinopyroxene inclusions in the IBM dunite sample are consistent with the typical partitioning between amphibole and clinopyroxene, which was probably accomplished by fractional crystallization (Fig. 6). This indicates that the clinopyroxene–pargasite inclusions crystallized from a melt, probably caused by the reaction specifically related to the depleted peridotite.

As shown in Fig. 3, the pargasites in the CIR samples and the MAR troctolite show flat to slightly LREE-enriched patterns, whereas the pargasites in the EPR sample show M-shaped LREE-depleted REE patterns. The compositions of residual peridotite also influenced the compositions of pargasites, although the contributions of evolved melt cannot be ignored. This can be inferred from the fact that residual peridotite from the EPR is more depleted than residual peridotite from the CIR and MAR, based on the spinel compositions (e.g., Dick and Natland 1996; Hellebrand et al. 2002; Tamura et al. 2008; Sanfilippo et al. 2015).

Implications and conclusions

Spinel-hosted hydrous mineral inclusions in the studied olivine-rich rocks are the products of reaction between melt and residual peridotite, and it is unlikely that they formed as a result of fractional crystallization of MORB melt beneath a mid-ocean ridge. The inclusions provide evidence for the participation of residual mantle peridotite in

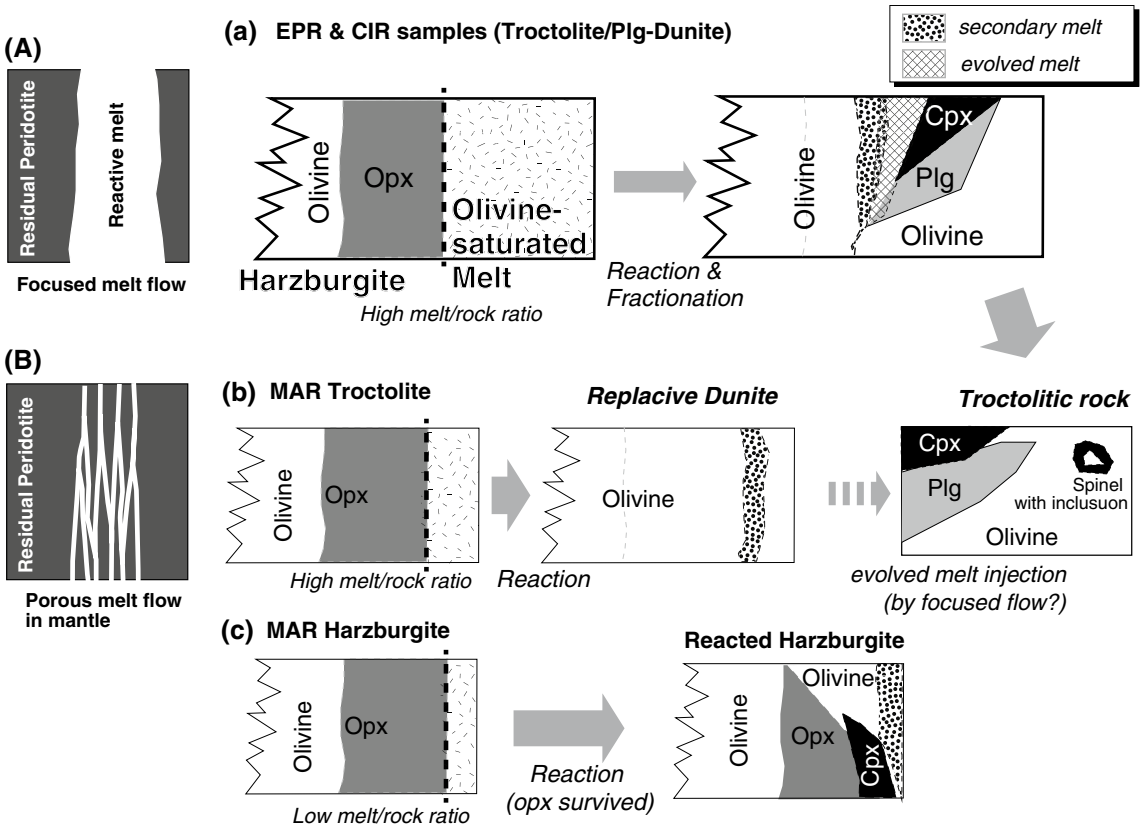

Fig. 7 Schematic cartoon of the classification of olivine-rich rocks formed in terms of reactions between residual harzburgite and olivine-saturated melt. Variations in the reactive melt flow (**A**, **B**) involved in the formation of olivine-rich rocks were expected from the melt/rock ratios in the reaction, based on the compositions of the spinel-hosted pargasite inclusions in the EPR and CIR samples (**a**) and MAR samples (**b**, **c**). Olivine-saturated melt corresponds to the reactive melt. The secondary melt, which was produced by incongruent melting of orthopyroxene (Opx) to crystallize olivine, contributed to the production of spinel with mineral inclusions. The crystallization of spinel can be enhanced by mixing the secondary melt with the olivine-saturated melt (e.g., Arai and Yurimoto 1994). (**a**) Reaction between harzburgite and a stagnant melt under high melt/rock ratios caused by focused melt flow (**A**). The secondary melt coexisted with and reacted with an evolved melt, which was produced separately by the fractionation of plagioclase (Plg) and clinopyroxene (Cpx) that followed on from olivine. The spinels with mineral inclusions were formed when the Plg and Cpx that make up the host troctolite crystallized. (**b**) Troctolitic rock formed from replacive dunite by the injection of a melt crystallizing Plag and Cpx. The replacive dunite with spinel-hosted mineral inclusions first began to form during reactions under porous melt flow in the mantle (**B**). (**c**) Melt-starving reaction with residual harzburgite. This example supports the proposition that the spinels with inclusions were produced by reactions between melt and residual harzburgite, such as during the formation of replacive dunite in (**b**) (Tamura et al. 2014)

the formation of the olivine-rich rocks and help distinguish them from rocks of cumulate origin. The trace-element compositions of the spinel-hosted pargasite inclusions are a reflection of whether or not the reactions between melt and residual peridotite progressed together with plagioclase crystallization. The diversities of the histories of formation of the olivine-rich rocks are responses to whether the reactions took place under porous melt flow (producing replacive dunite) or focused melt flow (accompanying fractional crystallization).

On the basis of the compositions of the spinel-hosted pargasite inclusions in the mid-ocean ridge samples, the variations in the ways the olivine-rich rocks formed are summarized in Fig. 7. As an example from the CIR and EPR samples, an evolved melt caused by plagioclase crystallization was involved during the decomposition of orthopyroxene in the residual peridotite, and the samples probably represent a crust–mantle boundary zone that was produced both by fractional crystallization of a MORB melt and by reaction of that melt with residual peridotite. Such a boundary zone is probably defined by the transition zone from porous melt flow in mantle peridotite to focused melt flow, where olivine-rich or gabbroic cumulates are formed by fractional crystallization of MORB melt (Fig. 7a). In contrast, the pargasite inclusions in the MAR troctolite were formed during the conversion of residual harzburgite to replacive dunite. This indicates that the formation of the MAR troctolite was initiated under porous melt flow in the mantle, prior to plagioclase crystallization (Fig. 7b). The MAR harzburgite was produced by an incomplete reaction

that formed replacive dunite (Fig. 7c), and the evidence from this sample supports the proposition that the formation of spinel-hosted mineral inclusions can be interpreted in terms of reactions between melt and residual peridotite (Tamura et al. 2014).

Accordingly, one troctolite sample was formed directly from the harzburgite together with gabbroic rocks by reactions between melt and harzburgite. This locally caused heterogeneities involving both mantle and crustal material. Another troctolite was created from replacive dunite by the further injection of melts that formed gabbroic rocks, and such replacive dunite consequently produced heterogeneities in the crustal material. This implies that the formation of replacive dunite in the mantle is sometimes obscured by the later formation of troctolite.

Acknowledgments We are grateful to the shipboard scientists, technicians, and specialists, as well as the captain and crew of the JOIDES Resolution and R/V Yokosuka, for collecting samples. This manuscript was revised following constructive comments from two reviewers and editorial comments by O. Müntener.

References

Akizawa N, Arai S, Tamura A (2012) Behavior of MORB magmas at uppermost mantle beneath a fast-spreading axis: an example from Wadi Fizh of the northern Oman ophiolite. Contrib Miner Petrol 164:601–625

Akizawa N, Ozawa K, Tamura A, Michibayashi K, Arai S (submitted) Three dimensional evolution of melting and heat/melt transfer in ascending mantle beneath a fast-spreading ridge segment constrained by trace elements of clinopyroxene in concordant dunites and host harzburgites of the Oman ophiolite. J Petrol

Arai S (1994) Characterization of spinel peridotites by olivine-spinel compositional relationships: review and interpretation. Chem Geol 113:191–204

Arai S, Abe N (1995) Reaction of orthopyroxene in peridotite xenoliths with alkali-basalt melt and its implication for genesis of alpine-type chromitite. Am Min 80:1041–1047

Arai S, Matsukage K (1996) Petrology of the gabbro–troctolite–peridotite complex from Hess Deep, equatorial Pacific: implications for mantle–melt interaction within the oceanic lithosphere. In: Mével C, Gillis KM, Allan JF, Meyer PS (eds) Proceedings of the ocean drilling program, scientific results 147. Ocean Drilling Program, College Station, pp 135–155

Arai S, Matsukage K (1998) Petrology of a chromitite micropod from Hess Deep, equatorial Pacific: a comparison between abyssal and alpine-type podiform chromitites. Lithos 43:1–14

Arai S, Miura M (2015) Podiform chromitites do form beneath mid-ocean ridges. Lithos 232:143–149

Arai S, Yurimoto H (1994) Podiform chromitites of the Tari–Misaka ultramafic complex, southwestern Japan, as mantle–melt interaction products. Econ Geol 89:1279–1288

Arai S, Matsukage K, Isobe E, Vysotskiy S (1997) Concentration of incompatible elements in oceanic mantle: effect of melt/wall interaction in stagnant or failed melt conduits within peridotite. Geochim Cosmochim Acta 61:671–675

Barns SJ, Roeder PL (2001) The range of spinel compositions in terrestrial mafic and ultramafic rocks. J Petrol 42:2279–2302

Coogan LA, Saunders AD, Kempton PD, Norry MJ (2000) Evidence from oceanic gabbros for porous melt migration within a crystal mush beneath the Mid-Atlantic Ridge. Geochem Geophys Geosyst 1. doi:10.1029/2000GC000072

Coogan LA, Wilson RN, Gillis KM, Macleod CJ (2001) Near-solidus evolution of oceanic gabbros: insights from amphibole geochemistry. Geochim Cosmochim Acta 65:4339–4357

Dick HJB, Natland JH (1996) Late-stage melt evolution and transport in shallow mantle beneath the East Pacific Rise. In: Mével C, Gillis KM, Allan JF, Meyer PS (eds) Proceedings of the ocean drilling program, scientific results, 147. Ocean Drilling Program, College Station, pp 103–134

Dick HJB, Natland JH, Ildefonse B (2006) Past and future impact of deep drilling in the oceanic crust and mantle. Oceanography 19:72–80

Dick HJB, Lissenberg CJ, Warren JM (2010) Mantle melting, melt transport, and delivery beneath a slow-spreading ridge: the paleo-MAR from 23°15′ N to 23°45′ N. J Petrol 51:425–467

Drouin M, Godard M, Ildefonse B (2007) Origin of olivine-rich troctolites from IODP Hole U1309D in the Atlantis Massif (Mid Atlantic Ridge): petrostructural and geochemical study. Eos Trans. AGU 88, Fall Meet. Supple: T53B-1300

Drouin M, Godard M, Ildefonse B, Bruguier O, Garrido CJ (2009) Geochemical and petrographic evidence for magmatic impregnation in the oceanic lithosphere at Atlantis Massif, Mid-Atlantic Ridge (IODP Hole U1309D, 30°N). Chem Geol 264:71–88

Drouin M, Ildefonse B, Godard M (2010) A microstructural imprint of melt impregnation in slow spreading lithosphere: olivine-rich troctolites from the Atlantis Massif, Mid-Atlantic Ridge, 30°N, IODP Hole U1309D, 30°N. Geochem Geophys Geosyst 11. doi:10.1029/2009GC002995

Elthon D, Matthew S, Kent RD (1992) Compositional trends of minerals in oceanic cumulates. J Geophys Res 97:15189–15199

Grove TL, Kinzler RJ, Bryan WB (1992) Fractionation of mid-ocean ridge basalt (MORB). In: Phipps-Morgan J, Blackman D, Sinton JM (eds) Mantle flow and melt generation at mid-ocean ridges. Geophysical monograph series. American Geophysical Union, Washington, pp 281–310

Gurenko AA, Chaussidon M (1995) Enriched and depleted primitive melts included in olivine from Icelandic tholeiites: origin by continuous melting of a single mantle column. Geochim Cosmochim Acta 59:2905–2917

Hellebrand E, Snow JE, Dick HJB, Hofman AW (2001) Coupled major and trace elements as indicators of the extent of melting in mid-ocean-ridge peridotites. Nature 410:677–681

Hellebrand E, Snow JE, Hoppe P, Hofmann A (2002) Garnet-field melting and late-stage refertilization in 'residual' abyssal peridotites from the Central Indian Ridge. J Petrol 43:2305–2338

Ildefonse B, Blackman DK, John BE, Ohara Y, Miller DJ, Macleod CJ, Abe N, Abratis M, Andal ES, Andréani M, Awaji S, Beard JS, Brunelli D, Charney AB, Christie DM, Delacour AG, Delius H, Drouin M, Einaudi F, Escartin J, Frost BR, Fryer PB, Gee JS, Godard M, Grimes CB, Halfpenny A, Hansen H-E, Harris AC, Hayman NW, Hellebrand E, Hirose T, Hirth JG, Ishimaru S, Johnson KTM, Karner GD, Linek M, Maeda J, Mason OU, Mccaig AM, Michibayashi K, Morris A, Nakagawa T, Nozaka T, Rosner M, Searle RC, Suhr G, Tamura A, Tominaga M, von der Handt A, Yamasaki T, Zhao X (2007) Oceanic core complexes and crustal accretion at slow-spreading ridges. Geology 35:623–626

Johnson KTM, Dick HJB, Shimizu N (1990) Melting in the oceanic upper mantle: an ion microprobe study of diopsides in abyssal peridotites. J Geophys Res 95:2661–2678

Kelemen PB, Shimizu N, Salters VJM (1995) Extraction of mid-ocean-ridge basalt from the upwelling mantle by focused flow of melt in dunite channels. Nature 375:747–753

Kelemen PB, Hirth G, Shimizu N, Spiegelman M, Dick HJB (1997) A review of melt migration processes in the asthenospheric mantle beneath oceanic spreading centers. Philos Trans R Soc Lond A 355:283–318

Matsukage K, Arai S (1998) Jadeite, albite and nepheline as inclusions in spinel of chromitite from Hess Deep, equatorial Pacific: their genesis and implications for serpentinite diapir formation. Contrib Miner Petrol 131:111–122

Morishita T, Ishida Y, Arai S, Shirasaka M (2005) Determination of multiple trace element compositions in thin (<30 μm) layers of NIST SRM 614 and 616 using laser ablation-inductively coupled plasma-mass spectrometry. Geostand Geoanal Res 29:107–122

Morishita T, Hara K, Nakamura K, Sawaguchi T, Tamura A, Arai S, Okino K, Takai K, Kumagai H (2009) Igneous, alteration and exhumation processes recorded in abyssal peridotites and related fault rocks from an oceanic core complex along the Central Indian Ridge. J Petrol 50:1299–1325

Morishita T, Tani K, Shukuno H, Harigane Y, Tamura A, Kumagai H, Hellebrand E (2011) Diversity of melt conduits in the Izu–Bonin–Mariana forearc mantle: implications for the earliest stage of arc magmatism. Geology 39:411–414

Morishita T, Nakamura K, Shibuya T, Kumagai H, Sato T, Okino K, Sato H, Nauchi R, Hara K, Takamaru R (2014) Petrology of peridotite and related gabbroic rocks around the Kairei hydrothermal field in the Central Indian Ridge. In: Ishibashi J-I et al (eds) Subseafloor biosphere linked to hydrothermal sysems: TAIGA concept. Springer, Tokyo, pp 177–193

Nakamura K, Morishita T, Chang Q, Neo N, Kumagai H (2007) Discovery of lanthanide tetrad effect in an oceanic plagiogranite from an Ocean Core Complex at the Central Indian Ridge 25oS. Geochem J 41:135–140

Nicolas A (1989) Structures of ophiolites and dynamics of oceanic crustal analogues. Kluwer, Dordrecht, p 367

Ozawa K, Shimizu N (1995) Open-system melting in the upper mantle: constraints from the Hayachine–Miyamori ophiolite, northern Japan. J Geophys Res 100:22315–22335

Parkinson IJ, Pearce JA (1998) Peridotites from the Izu–Bonin–Mariana forearc (ODP Leg 125): evidence for mantle melting and melt–mantle interaction in a supra-subduction zone setting. J Petrol 39:1577–1618

Renna MR, Tribuzio R (2011) Olivine-rich troctolites from Ligurian ophiolites (Italy): evidence for impregnation of replacive mantle conduits by MORB-type melts. J Petrol 52:1763–1790

Reynolds JR, Langmuir CH (1997) Petrological systematics of the Mid-Atlantic Ridge south of Kane: implications for ocean crust formation. J Geophys Res 102:14915–14946

Roeder PL, Reynolds I (1991) Crystallization of chromite and chromium solubility in basaltic melts. J Petrol 32:909–934

Sanfilippo A, Tribuzio R (2013a) Origin of the olivine-rich troctolites from the oceanic lithosphere: a comparison between the alpine Jurassic ophiolite and modern slow spreading ridges. Ofioliti 38:91–101

Sanfilippo A, Tribuzio R (2013b) Building of the deepest crust at a fossil slow-spreading centre (Pineto gabbroic sequence, alpine Jurassic ophiolites). Contrib Miner Petrol 165:705–721

Sanfilippo A, Dick HJB, Ohara Y (2013) Melt-rock reaction in the mantle: mantle troctolites from the Parece Vela ancient back-arc spreading center. J Petrol 54:861–885

Sanfilippo A, Morishita T, Kumagai H, Nakamura K, Okino K, Hara K, Tamura A, Arai S (2015) Hybrid troctolites from mid-ocean ridges: inherited mantle in the lower crust. Lithos 232:124–130

Schiano P, Clocchiatti R, Lorand J-P, Massare D, Deloule E, Chaussidon M (1997) Primitive basaltic melts included in podiform chromites from the Oman ophiolite. Earth Planet Sci Lett 146:489–497

Shaw CSJ (1999) Dissolution of orthopyroxene in basanitic magma between 0.4 and 2 GPa: further implications for the origin of Si-rich alkaline glass inclusions in mantle xenoliths. Contrib Miner Petrol 135:114–132

Shaw CSJ, Thibault Y, Edgar AD, Lloyd FE (1998) Mechanisms of orthopyroxene dissolution in silica-undersaturated melts at 1 atmosphere and implications for the origin of silica-rich glass in mantle xenoliths. Contrib Miner Petrol 132:354–370

Shimizu K, Komiya T, Hirose K, Shimizu N, Maruyama S (2001) Cr-spinel, an excellent micro-container for retaining primitive melts—implications for a hydrous plume origin for komatiites. Earth Planet Sci Lett 189:177–188

Su B-X, Zhang H-F, Yang Y-H, Sakyi P, Ying J-F, Tang Y-J (2012) Breakdown of orthopyroxene contributing to melt pockets in mantle peridotite xenoliths from the Western Qinling, central China: constraints from in situ LA–ICP–MS mineral analyses. Miner Petrol 104:225–247

Suhr G, Hellebrand E, Johnson K, Brunelli D (2008) Stacked gabbro units and intervening mantle: a detailed look at a section of IODP Leg 305, Hole U1309D. Geochem Geophys Geosyst 9. doi:10.1029/2008GC002012

Sun SS, Mcdonough WF (1989) Chemical and isotopic systematics of oceanic basalts: implications for mantle composition and processes. In: Saunders AD, Norry MJ (eds) Magmatism in the ocean basins. Geological society special publication 42. Geological Society, London, pp 313–345

Tamura A, Arai S (2006) Harzburgite–dunite–orthopyroxenite suite as a record of supra-subduction zone setting for the Oman ophiolite mantle. Lithos 90:43–56

Tamura A, Arai S, Ishimaru S, Andal E (2008) Petrology and geochemistry of peridotites from IODP Site U1309 at Atlantis Massif, MAR 30°N. Contrib Mineral Petrol 155:491–509

Tamura A, Morishita T, Ishimaru S, Arai S (2014) Geochemistry of spinel-hosted amphibole inclusions in abyssal peridotite: insight into secondary melt formation in melt–peridotite reaction. Contrib Miner Petrol 167:1–16

Umino S, Kitamura K, Kanayama K, Tamura A, Sakamoto N, Ishizuka O, Arai S (2015) Thermal and chemical evolution of the subarc mantle revealed by spinel-hosted melt inclusions in boninite from the Ogasawara (Bonin) Archipelago, Japan. Geology 43:151–154

Zhou MF, Robinson PT, Bai WJ (1994) Formation of podiform chromitites by melt/rock interaction in upper mantle. Miner Depos 29:98–101